




Unveiling the robustness of porphyrin crystalline nanowires toward aggressive chemicals

L. Fazi¹, L. Raimondo², B. Bonanni¹, M. Fanfoni¹, R. Paolesse³, A. Sgarlata¹, A. Sassella², C. Goletti^{1,a} 

¹ Dipartimento di Fisica, Università di Roma “Tor Vergata”, Via della ricerca scientifica 1, 00133 Rome, Italy

² Dipartimento di Scienza dei Materiali, Università di Milano - Bicocca, Via Cozzi 55, 20125 Milan, Italy

³ Dipartimento di Scienze e Tecnologie Chimiche, Università di Roma “Tor Vergata”, Via della ricerca scientifica 1, 00133 Rome, Italy

Received: 1 September 2021 / Accepted: 3 February 2022

© The Author(s) 2022, corrected publication 2022

Abstract One of the keys for the development of porphyrin-based devices implies that their functionality must be robust and stable against external environmental factors. While the research has been mostly focused on the supramolecular aggregate interactions with target chemicals, the robustness of organic nanostructures in contaminating and even aggressive environments has not been diffusely investigated yet. The results here presented show that crystalline nanowires of *meso*-tetraphenyl porphyrin (H₂TPP) and *meso*-tetraphenyl porphyrin-Zn(II) (ZnTPP) are insensitive to the exposure to a series of purposely chosen analytes (alcohols, alkanes and amines). Our finding suggests possible applications of the nanowires in organic-based devices (overwhelming the well-known intrinsic weakness of organic electronics), related to material stability through an appropriate material design and the opportunity offered by organic epitaxy.

1 Introduction

The fascinating world of porphyrins offers almost unlimited opportunities of exploiting the richness of their properties in view of nanotechnological applications, tailoring the molecular systems by appropriate peripheral decorations of the single molecule, as well as by the assembly of molecular units in complex architectures [1]. Ordered or disordered layers, nanoparticles, nanosheets, nanorods, nanorings, nanowires, and nanotubes have been prepared, characterized, and applied in photocatalysis, pharmacology, solar energy conversion, sensors, and hybrid devices [2–9]. In view of their use in these different fields, various characteristics of the porphyrin-based molecular structures have been studied: to mention some examples, the sensitivity and/or selectivity to target analytes [10], the transport dependence upon the size of the nanostructures [11], the effect of charging and discharging processes in varying the conductance of a field-effect transistor [12]. Porphyrins in these devices have an active role: their tunable reactivity on one side represents the main reason for application in sensors [13], but on the other side it can limit their stability, since they suffer photobleaching, solvolysis by the solvent, or damage after exposure to aggressive analytes [14]. This reduced stability can consequently produce a gradual loss of the efficiency, and a worsening of the device performance.

The driving force for the porphyrin self-organization in the solid state is mainly the π – π stacking interaction between the planar aromatic rings, which represents an excellent platform for organizing the ordered aggregation at the nanoscale. These π – π stackings are considered as weak interactions in supramolecular chemistry, but their synergy can produce stable structures, insoluble in common solvents, for example observed in porphyrin or octamethylporphyrin. The ordered aggregation of porphyrins can be achieved in different ways, but an extremely high control level in building up nanostructures is possible by using organic epitaxy, i.e., by the deposition of molecules on appropriately chosen organic substrates driving the crystal structure and orientation of the organic layer [7, 15–17]. Among supramolecular nanostructures, nanowires represent an intriguing choice for wiring elements in organic devices and circuits at the nanoscale [12, 18]. For example, it has been demonstrated that nanowires of fused-oligo-porphyrins exhibit a negative attenuation factor of conductivity with length [19], differently from single molecule wires [20], although the better transport properties of the former are accompanied by a higher reactivity versus analytes, as the nanowires expose directly the naked core of the ring.

In the last years, the use of porphyrin aggregates and nanostructures for sensing applications has represented a significant achievement in constructing solid-state devices for the detection and recognition of volatiles [10, 21]. By exploiting: (1) the supramolecular chemistry to assemble molecules; (2) the flexibility of porphyrins to tune their molecular properties; and (3) the richness of such properties, complex architectures have been obtained, with a higher sensitivity to analytes and a larger range of applications compared to single molecular units [10]. Porphyrins can bind target analytes with a manifold of different interactions, ranging from the axial binding to the coordinated metal to end with the unavoidable dispersion forces. In nano-gravimetric chemical sensors [13],

^a e-mail: goletti@roma2.infn.it (corresponding author)

all these porphyrin-analyte bonding interactions lead to the increase of mass of the sensing layer that causes a characteristic shift of the resonance frequency of the oscillating quartz (where the porphyrin have been deposited), thus transducing the adsorption of gaseous particles in an electric signal. This signal is directly connected to the modifications of the optical anisotropy of the porphyrin layer, indeed sensitive to structural/chemical modifications [22]. By depositing metalloporphyrins onto solid substrates, as demonstrated for Langmuir–Schaeffer (LS) and Langmuir–Blodgett (LB) films, monitoring of the adsorption of analytes can be carried out by optical methods using polarized light, namely by reflectance anisotropy spectroscopy (RAS) [22, 23]. RAS has enabled the identification of classes of molecules (alcohols, alkanes, amines) on the basis of the interaction involved in the adsorption process, resulting in a signal linearly connected to the composition of the analyzed atmosphere [23].

Within this frame, the present study is aimed at checking by optical measurements if specific, highly ordered, crystalline nanostructures, namely crystalline nanowires of *meso*-tetraphenyl porphyrin (H_2TPP) and *meso*-tetraphenyl porphyrin-Zn(II) (ZnTPP), may interact with different analytes, given their crystal structure where the molecules are closely packed. The choice of these two molecules has permitted investigating the effects of the insertion of a coordinated metal atom in the porphyrin center to favor a stronger coordination interaction with analytes, as indeed happens in amines. Then, depending on the level of reactivity, such nanowires may be assessed as more or less adequate, to act as functional materials in sensors or other organic electronic devices [24]. In other words, the present paper can also bestow a conceivable extension of the application of porphyrins nanowires beyond sensors, in particular, in aggressive environment.

2 Experimental

Meso-tetraphenyl porphyrin (H_2TPP) and *meso*-tetraphenyl porphyrin-Zn(II) (ZnTPP) (Sigma-Aldrich) were used as received. (010)-oriented single crystals of potassium acid phthalate (KAP) were purchased from Ekspla to be used as substrates and were cleaved in air before use. Thin films of H_2TPP and ZnTPP were grown at room temperature on KAP substrates by means of an organic molecular beam epitaxy (OMBE) apparatus working under high vacuum (base pressure $< 2 \times 10^{-7}$ torr) with a Knudsen-type effusion cell at 275 °C for H_2TPP and 307 °C for ZnTPP.

Films of two different *nominal* thicknesses, 3 nm and 5 nm, were grown for each molecule. The nominal thickness was monitored by means of a quartz microbalance. According to the growth protocols reported in Refs. [7, 26], H_2TPP and ZnTPP crystalline nanowires are selectively grown, uniformly distributed over the whole substrate surface. Atomic force microscopy (AFM) images were collected in intermittent-contact mode in air with a Nanoscope V MultiMode (Bruker) microscope, with silicon probes (tip radius 8 nm, spring constant 40 N/m, resonance frequency ≈ 340 kHz) with a resolution of 512×512 pixels. Image processing was performed with the software WSXM [25]. In Fig. 1, the surface of two 5-nm-thick films is shown, as imaged by AFM, and shows the presence of the nanowires. The crystal structure of the nanowires is a specific polymorph of the two materials, having in both cases the stacking direction of the molecules along the long wire axis, which results well aligned along $[001]_{KAP}$, thanks to organic epitaxy [7, 26]. A detailed discussion about the growth protocol, structural characterization, and epitaxial relation is reported in Refs. [7, 26].

After growth, the samples have been inserted in a little stainless steel chamber with inlet and outlet gates for the gas flow, controlled by valves. In stationary conditions (that is without analytes entering the chamber), the inner atmosphere of the chamber was high purity (99.999%) nitrogen. A home-made glass window allows the normal-incidence optical access to the sample, kept at room temperature. The optical measurements have been performed measuring the optical anisotropy by a RAS spectrometer in the range 250–800 nm, using a Xe lamp, a grating monochromator, two CaF_2 Glan–Taylor polarizers, a photoelastic modulator (PEM), and a photomultiplier as detector [27].

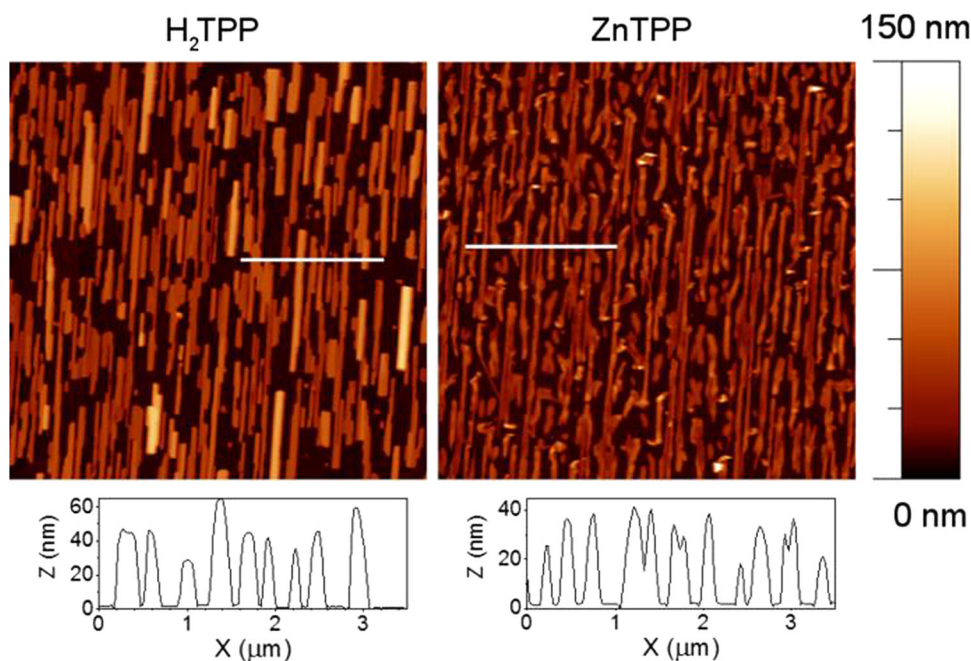
In RAS one measures, at nearly normal incidence, the difference of the sample reflectance (ΔR) for light linearly polarized alternatively along two perpendicular directions (α and β), then reporting the ratio between ΔR and the average sample reflectance (R) as a function of wavelength:

$$\Delta R/R = 2(R_\alpha - R_\beta)/(R_\alpha + R_\beta)$$

where R_i ($i = \alpha, \beta$) is the reflectance for linearly polarized light in state i . The RAS technique (applied to inorganic surfaces [28], organic materials [29–33], 2D materials [34]) is discussed in details elsewhere [35]; it is important to note here its extremely high sensitivity, up to 1×10^{-5} . When a signal is measured, however, the detection chain (preamplifier and digital lock-in) has to be set at the proper scale, so that in conclusion variations as low as 1×10^{-2} of the anisotropy signal itself can be measured. In our experiment, the electric field of light was linearly polarized, respectively, parallel (α) and orthogonal (β) to the long axis of the nanowires, i.e., the direction of the maximum optical anisotropy of the film [7, 26].

We have monitored the RAS signal during the exposure of the film to vapors of different chemical species. Vapors were obtained by N_2 bubbling at room temperature in the liquid analyte, and injected into the measurement cell. As analytes, two alcohols (ethanol, butanol), two amines (butylamine, triethylamine), and an alkane (hexane) were considered. This choice has been done to investigate the different interaction modes among porphyrin nanowires and volatiles. For hexane only London forces can occur, while in the case of alcohols both coordination to the metal ion and hydrogen bond are added. In the case of amines, the coordination to Zn ion is enhanced as a strong interaction. For alcohols, the two compounds have been tested to evaluate the possible influence of the

Fig. 1 AFM $5\ \mu\text{m} \times 5\ \mu\text{m}$ height images of (left panel) a 5-nm-thick H_2TPP film on KAP, and (right panel) a 5-nm-thick ZnTPP film on KAP. Both films are made of crystalline nanowires, well aligned along the [001] direction of the KAP substrate, obtained following specific growth protocols. Below each image, the signal profile collected along the white line is also reported



dispersion interaction related to the length of alkyl chain. Finally, we used both amines, because the linear structure of butylamine can avoid the steric effect present when the bulky triethylamine interacts with the porphyrin aggregates in the solid layer.

To monitor the variations of $\Delta R/R$ eventually produced by interaction of the nanowires with the analytes, the following procedure has been adopted for all samples:

- The RAS spectrum in the 350–650 nm spectral range (350–500 nm for ZnTPP) has been recorded *before* and *after* exposure, and the difference calculated to highlight signal variations; the “*before*” spectrum relates to the film *as grown* and stored in atmosphere;
- During each exposure stage, the RAS signal has been monitored in time every 10 s—intervals at fixed photon wavelength (usually selecting the maximum of the $\Delta R/R$ curve).

After each exposure stage, the effect of purging by a flux of pure nitrogen in the chamber, known to remove the contaminants recovering the original film conditions, was also monitored by RAS.

3 Results and discussion

In Fig. 2, the RAS spectra of two as-grown films of H_2TPP (black curve) and ZnTPP (red curve), deposited on KAP with 5 nm nominal thickness, are presented. The peak of the anisotropy (430 nm for H_2TPP and 447 nm for ZnTPP) is for both materials in the spectral range of the Soret bands, dominating the UV–Vis spectrum of porphyrins crystals [7, 26, 36]. The spectra for the 3-nm-thick samples are similar, with lower amplitude. In all cases, the anisotropy reaches remarkable values, as high as about 50–70% for the thicker layers. The high anisotropy values are consistent with the optical anisotropy observed using polarized light transmission spectra measured with the light electric field parallel and perpendicular to the long nanowire axis [26, 36]. At longer wavelengths, characteristic oscillations dominate all the spectra: they are due to the KAP birefringence, as the polarization axes of the spectrometer do not coincide perfectly with the symmetry axes of KAP [27].

Exposure to alcohol has been already demonstrated to lead to detectable variations of the anisotropy signal in the visible–UV region in porphyrins [37]. Monitoring the RAS response of the H_2TPP and ZnTPP nanowires during exposure to ethanol and butanol permits checking the strength and characteristics of the interaction resulting with these porphyrins when they are in the form of crystalline nanowires with the specific structure. When ethanol and butanol are compared, the main common interactions with porphyrin layers are the non-selective London forces, with the addition of H bonds for H_2TPP and coordination for the ZnTPP layer. However, the longer carbon chain of butanol increases the importance of non-selective dispersion forces with respect to the more selective H bond and coordination interactions.

In Fig. 3, we report a representative series of the results obtained exposing the 3-nm-thick film of H_2TPP to ethanol and butanol, being paradigmatic of the behavior of all the other samples. In Fig. 3, (left panel) the spectra collected before (red curve) and after (green curve) exposure are reported, almost indistinguishable; this is confirmed by the difference spectrum (black curve), which

Fig. 2 $\Delta R/R$ spectra measured at two films on KAP with the same nominal thickness of 5 nm: a film of H₂TPP (black curve) and a film of ZnTPP (red curve). The positive peak means higher reflectance for light polarized along the nanowire axis. The low energy side of the anisotropy peak for H₂TPP is dominated by oscillations (due to the birefringence of the KAP substrate, as explained in Ref. [27]), that obscure almost completely the presence of any other structure. Consequently, for ZnTPP $\Delta R/R$ spectra have been measured in a limited wavelength range, without losing any significant information

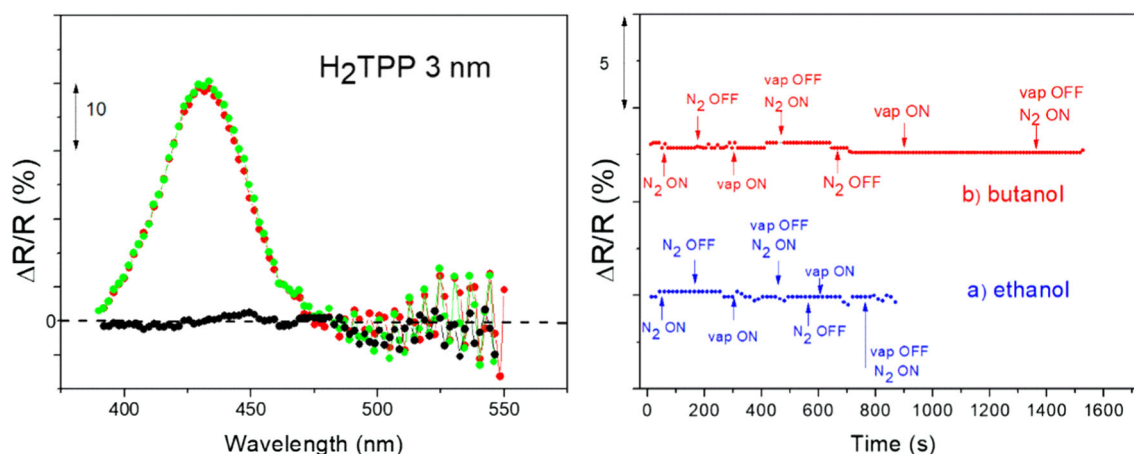
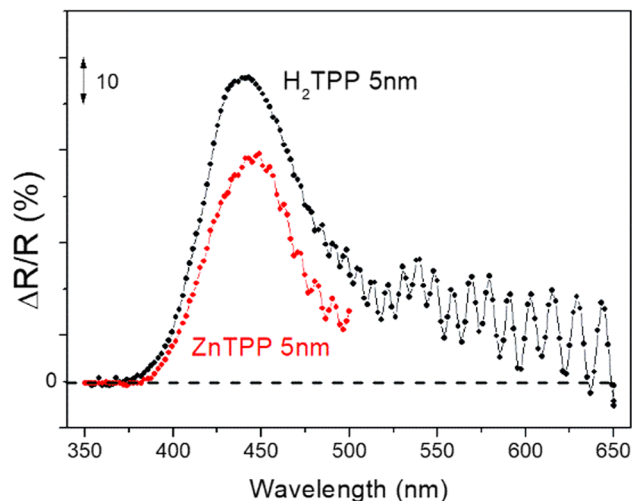


Fig. 3 Left panel: $\Delta R/R$ spectra measured at a 3-nm-thick H₂TPP film before (red curve) and after (green curve) exposure to saturated vapors of ethanol. The black curve represents the difference between the two spectra. Right panel: RAS signal measured at the peak position (430 nm) of the $\Delta R/R$ spectrum of the same film during exposure to saturated vapors of ethanol and butanol ($p_{\text{eth}} = 5.73 \text{ kPa @ 293 K}$; $p_{\text{but}} = 1.7 \text{ kPa @ 293 K}$). The arrows indicate when the purging N₂ gas and the analyte vapor (vap) have been introduced (ON) or not (OFF) in the chamber. The signals have been arbitrarily shifted on the vertical axis to present them in the same plot

results in a nearly zero line (the oscillations above 460 nm originate from the not-coincident KAP-related fringes, being therefore meaningless in terms of evolution with vapor exposure).

These results demonstrate the insensitivity to alcohols of all nanowire samples, independently of the molecules, H₂- or Zn-TPP, and film thickness. Strong support to this conclusion comes from the data in the right panel of Fig. 3, showing the optical signal of the same sample at 430 nm, monitored during exposure and purging cycles with the different alcohols. Introduction of the analyte (vapor ON) is followed by cleaning cycles (vapor OFF, nitrogen ON), leaving the RAS signal almost unchanged; the tiny ($< 5 \times 10^{-3}$) and irregular variations of the signal sometimes recorded (not correlated to the gas inlet) correspond to the *noise* at the chosen scale of the electronic chain detecting the modulated RAS signal. A similar “negative” behavior is observed for both alcohols and all the different samples. This result is at variance with previous experiments by RAS on LB layers of porphyrins, where a clear modification (about one tenth of the whole anisotropy) of the spectral line shape is observed around the Soret band during exposure to well lower quantities of ethanol [37]. In that case, the quite fast and reversible variation of the optical anisotropy has been explained in terms of a temporary structural modification of the film.

In Fig. 4, the response to hexane of the 5-nm-thick ZnTPP film, taken as an example representative for all samples, is shown in terms of the same curves as those in Fig. 3: in the left panel, the spectra before and after exposure are reported, while the right panel shows the signal at 447 nm during several cycles. Once more, the spectra and their difference do not permit observation of any variation upon exposure to hexane vapor; at the same time, the signal at 447 nm does not exhibit any meaningful variation. Some differences with respect to the previous case could in principle be expected between H₂- and Zn-TPP: with ethanol and butanol multiple binding mechanisms, such as hydrogen bond or coordination to the porphyrin core metal can be present, while hexane can only be adsorbed via dispersion interactions.

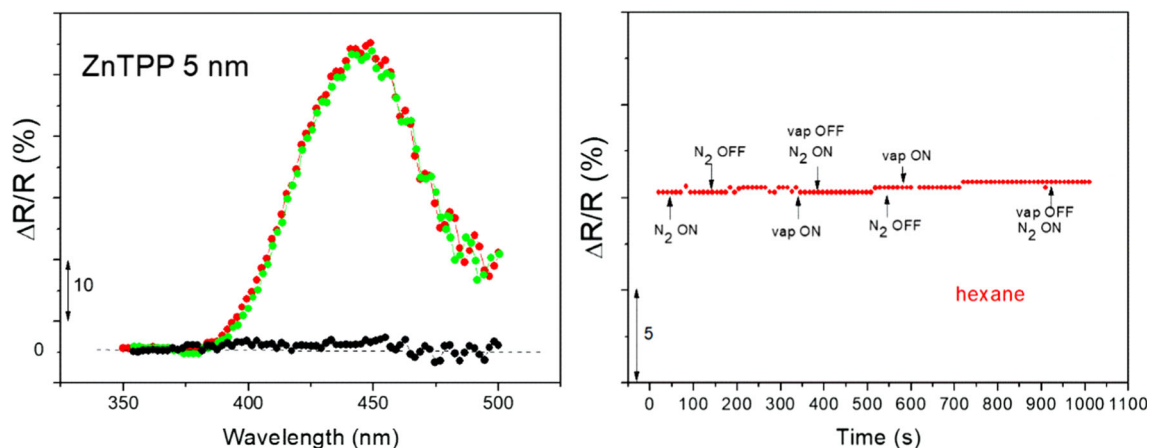


Fig. 4 Left panel: $\Delta R/R$ spectra measured at a 5-nm-thick ZnTPP film before (red curve) and after (green curve) exposure to saturated vapors of hexane ($p_{\text{hex}} = 16.94 \text{ kPa}@300 \text{ K}$). The two spectra are almost perfectly superimposed. The black curve represents the difference between the two spectra. Right panel: RAS signal measured at the peak position (447 nm) of the $\Delta R/R$ spectrum of the same film during exposure to saturated vapors of hexane. The arrows indicate when the purging N_2 gas and the analyte vapor (vap) have been introduced (ON) or not (OFF) in the chamber

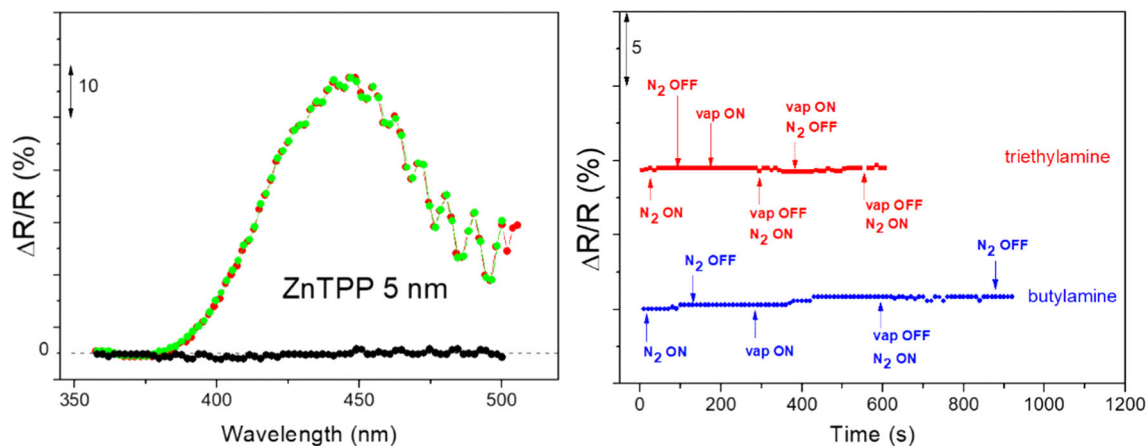


Fig. 5 Left panel: $\Delta R/R$ spectra measured at a 5-nm-thick ZnTPP film before (green curve) and after (red curve) exposure to saturated vapors of butylamine. The two spectra are almost perfectly superimposed. The black curve represents the difference between the two spectra. Right panel: RAS signal measured at the peak position (447 nm) of the $\Delta R/R$ spectrum of a 5-nm-thick ZnTPP nanowires film during exposure of the film to saturated vapors of triethylamine (red curve, $p_{\text{triethy}} = 6.9 \text{ kPa} @ 293 \text{ K}$) and butylamine (blue curve, $p_{\text{buthy}} = 10.9 \text{ kPa} @ 293 \text{ K}$). The arrows indicate when the purging N_2 gas and the analyte vapor (vap) have been introduced (ON) or not (OFF) in the chamber

This noteworthy lack of sensitivity versus the chosen set of chemicals definitely rules out the possible use of our porphyrin crystalline nanowires as active elements in gas sensors, contrary to layers, nanosheets, or nanotubes displaying a completely different molecular packing [2–6]. The detected insensitivity of the nanowires versus the analytes is not due to the molecule, being present in all mentioned structures, nor to the length and density of the nanowires. In fact, their crystal structure hinders the mechanisms of binding between the analytes and the molecules, thanks to a closely packed arrangement of the molecules in the crystal, like in a Roman “testudo” formation. The distance between two adjacent H_2TPP porphyrin molecules in an ordered structure due to π – π interaction varies in a range [38] whose average nicely compares with the stacking distance along the nanowire of the same molecule (3.79 Å), coming from the peculiar crystal structure [7]. When the analytes interact with porphyrins through the known, various mechanisms, the effect of the different interactions can be dramatically dissimilar: while the low energy dispersion interactions can induce swelling of the nanostructure, with the macrocycles slightly moving away from each other, the coordination of analytes completely destroys the three-dimensional structure of the nanowire, because it imposes the separation of the vicinal porphyrin disks; in this case, the *stiffness* of the whole nanowire structure due to the supramolecular organization in the crystal can prevent the interaction, which would have a very high energetic cost (larger than for a simple couple of paired porphyrins). This is at variance with LB or LS layers exposed to gases or vapors [22, 23]: in these cases, the less strongly packed structure of the porphyrin assembly is prone to favor the interaction of molecules with analytes.

The same series of experiments have been repeated for all the samples with two amines, namely triethylamine and butylamine, both of them expected to have a coordination interaction with the Zn ion, similar to alcohols and hexane, but with a stronger intensity. The experiments result in an evident lack of any effect on the optical anisotropy of the nanowires, also in the case of ZnTPP (expected

to have a stronger interaction). We present in Fig. 5 the signal monitored on a 5-nm-thick ZnTPP film at about 447 nm during the two distinct exposure stages, displaying a conclusive and unexpected, given the strong reactivity of amines, absence of effects.

4 Conclusions

The results here shown clearly demonstrate that the crystalline H₂TPP or ZnTPP nanowires grown by OMBE on a properly selected crystalline substrate present a completely different behavior with respect to most porphyrin aggregates and nanostructures, being insensitive to the presence of different analytes. Therefore, the exploitation of these nanowires as sensing elements in chemical sensors *cannot* be proposed: the compact structure of the nanowire eliminates any possibility of interaction with analytes, preventing, in the case of ZnTPP, even the strong coordination of butylamine with the metal ion, otherwise causing the swelling of the structure. On the contrary, the robustness of these nanowires even in very aggressive environments suggests a possible application as active materials in organic devices, to overwhelm their intrinsic weakness related to the limited material stability [24]. As a more general conclusion, our work demonstrates that organic molecular nanostructures suitable for device integration, such as our crystalline TPP nanowires, can be implemented through an appropriate material design by taking advantage of the opportunity offered by organic epitaxy, thus achieving a real molecular architectonics for functional applications.

Acknowledgements R.P. and C.G. thank the University of Rome Tor Vergata for funding ("Mission Sustainability 2017" SensAir project E81I18000180005). A.S. and L.R. thank the University of Milano Bicocca for funding (Bando Infrastruttura di Ricerca 2021).

Funding Open access funding provided by Università degli Studi di Roma Tor Vergata within the CRUI-CARE Agreement.

Data Availability Statement This manuscript has associated data in a data repository. [Authors' comment: All the data included in this study are available from the corresponding author upon reasonable request.]

Open Access This article is licensed under a Creative Commons Attribution 4.0 International License, which permits use, sharing, adaptation, distribution and reproduction in any medium or format, as long as you give appropriate credit to the original author(s) and the source, provide a link to the Creative Commons licence, and indicate if changes were made. The images or other third party material in this article are included in the article's Creative Commons licence, unless indicated otherwise in a credit line to the material. If material is not included in the article's Creative Commons licence and your intended use is not permitted by statutory regulation or exceeds the permitted use, you will need to obtain permission directly from the copyright holder. To view a copy of this licence, visit <http://creativecommons.org/licenses/by/4.0/>.

References

1. M.B. Avinash, T. Govindaraju, *Acc. Chem. Res.* **51**, 41 (2018)
2. S. Watcharinyanon, D. Nilsson, E. Moons, A. Shaporenko, M. Zharnikov, B. Albinsson, J. Martensson, L.S.O. Johansson, *Phys. Chem. Chem. Phys.* **10**, 5264 (2008)
3. X. Gong, T. Milic, C. Xu, J.D. Batteas, C.M. Drain, *J. Am. Chem. Soc.* **124**, 14290 (2002)
4. Y. Tian, C.M. Beavers, T. Busani, K.E. Martin, J.L. Jacobsen, B.Q. Mercado, B.S. Swartzentruber, F. van Swol, C.J. Medforth, J.A. Shelnutt, *Nanoscale* **4**, 1695 (2012)
5. D. Laurencin, P.G. Yot, C. Gervais, Y. Guari, S. Clément, E. Elkaim, M. Paillet, D. Didier Cot, S. Richeter, *Porphyrin Science by Women* (World Scientific, Singapore, 2021), p. 915
6. C. Maeda, S. Toyama, N. Okada, K. Takaishi, S. Kang, D. Kim, T. Ema, *J. Am. Chem. Soc.* **142**(37), 15661 (2020)
7. M. Campione, G.C. Capitani, L. Raimondo, A. Sassella, *J. Phys. Chem. C* **119**, 18210 (2015)
8. R. Havera, H.L. Anderson, *Helv. Chim. Acta* **102**, e1800211 (2019)
9. Y. Chen, A. Li, Z.H. Huang, L.N. Wang, F. Kang, *Nanomaterials* **6**, 51 (2016)
10. C. Di Natale, D. Monti, R. Paolesse, *Mater. Today* **13**, 46–52 (2010)
11. T. Kim, S. Ham, S.H. Lee, Y. Honga, D. Kim, *Nanoscale* **10**, 16438 (2018)
12. M. Seol, S. Choi, C. Kim, D. Moon, Y. Choi, *ACS Nano* **6**, 183–189 (2012)
13. R. Paolesse, S. Nardis, D. Monti, M. Stefanelli, C. Di Natale, *Chem. Rev.* **117**, 2517 (2017)
14. U. Bazylińska, R. Frąckowiak, Z. Brzózka, K.A. Wilk, *J. Photochem. Photobiol. B Biol.* **166**, 169 (2017)
15. D.E. Hooks, T. Fritz, M.D. Ward, *Adv. Mater.* **13**, 227 (2001)
16. G. Koller, S. Berkebile, J.R. Krenn, F.P. Netzer, M. Oehzelt, T. Haber, R. Resel, M.G. Ramsey, *Nano Lett.* **6**, 1207 (2006)
17. M. Campione, A. Sassella, M. Moret, A. Papagni, S. Trabatonni, R. Resel, O. Lengyel, V. Marcon, G. Raos, *J. Am. Chem. Soc.* **128**, 13378 (2006)
18. S.T. Schneebeli, M. Kamenetska, Z. Cheng, R. Skouta, R.A. Friesner, L. Venkataraman, R. Breslow, *J. Am. Chem. Soc.* **133**, 2136 (2011)
19. N. Algethami, H. Sadeghi, S. Sangtarash, C.J. Lambert, *Nano Lett.* **18**, 4482 (2018)
20. S. Sangtarash, A. Vezzoli, H. Sadeghi, N. Ferri, H.M. O'Brien, I. Grace, L. Bouffier, S.J. Higgins, R.J. Nichols, C.J. Lambert, *Nanoscale* **10**, 3060 (2018)
21. E.A. Kuposova, A. Offenhäusser, Y.E. Ermolenko, Y.G. Mourzina, *Front. Chem.* **7**, 351 (2019)
22. G. Bussetti, S. Cirilli, A. Violante, P. Chiaradia, C. Goletti, L. Tortora, R. Paolesse, E. Martinelli, A. D'Amico, C. Di Natale, G. Giancane, L. Valli, *Appl. Phys. Lett.* **95**, 091906 (2009)
23. G. Bussetti, A. Violante, R. Yivlialin, S. Cirilli, B. Bonanni, P. Chiaradia, C. Goletti, L. Tortora, R. Paolesse, E. Martinelli, A. D'Amico, C. Di Natale, G. Giancane, L. Valli, *J. Phys. Chem. C* **115**, 8189 (2011)
24. E.K. Lee, M.Y. Lee, C.H. Park, H.R. Lee, J.H. Oh, *Adv. Mater.* **29**, 1703638 (2017)
25. I. Horcas, R. Fernández, J.M. Gómez-Rodríguez, J. Colchero, J. Gómez-Herrero, A.M. Baro, *Rev. Sci. Instrum.* **78**, 013705 (2007)

26. L. Raimondo, S. Trabattoni, A. Sassella, Phys. Chem. Chem. Phys. **21**, 8482 (2019)
27. C. Goletti, G. Bussetti, P. Chiaradia, A. Sassella, A. Borghesi, Appl. Phys. Lett. **83**, 4146 (2003)
28. G. Bussetti, C. Goletti, P. Chiaradia, T. Derry, Europhys. Lett. **79**, 57002 (2007). (**and references therein**)
29. G. Bussetti, S. Cirilli, A. Violante, V. Chiostrì, C. Goletti, P. Chiaradia, A. Sassella, M. Campione, L. Raimondo, D. Braga, A. Borghesi, J. Vacuum Sci. Technol. A **27**, 1029 (2009)
30. M. Campione, A. Borghesi, M. Laicini, A. Sassella, C. Goletti, G. Bussetti, P. Chiaradia, J. Chem. Phys. **127**, 244703 (2007)
31. A. Sassella, M. Campione, L. Raimondo, A. Borghesi, G. Bussetti, S. Cirilli, A. Violante, C. Goletti, P. Chiaradia, Appl. Phys. Lett. **94**, 073307 (2009)
32. B.G. Frederick, J.R. Power, R.J. Cole, C.C. Perry, Q. Chen, S. Haq, Th. Bertrams, N.V. Richardson, P. Weightman, Phys. Rev. Lett. **80**, 4490 (1998)
33. A. Navarro-Quezada, E. Ghanbari, T. Wagner, P. Zeppenfeld, J. Phys Chem C **122**, 12704 (2018)
34. R. Denk, M. Hohage, P. Zeppenfeld, J. Cai, C.A. Pignedoli, H. Söde, R. Fasel, X. Feng, K. Müllen, S. Wang, D. Prezzi, A. Ferretti, A. Ruini, E. Molinari, P. Ruffieux, Nat. Commun. **5**, 4253 (2014)
35. P. Weightman, D.S. Martin, R.J. Cole, T. Farrell, Rep. Prog. Phys. **68**, 1251 (2005)
36. M. Palumbo, L. Raimondo, C. Hogan, C. Goletti, S. Trabattoni, A. Sassella, J. Phys. Chem. Lett. **12**, 869 (2021)
37. G. Bussetti, C. Corradini, C. Goletti, P. Chiaradia, M. Russo, R. Paolesse, C. Di Natale, A. D'Amico, L. Valli, Phys. Stat. Sol. (B) **242**, 2714 (2005)
38. M.O. Senge, in *The Porphyrin Handbook*, vol. 10, ed. by K.M. Kadish, K.M. Smith, R. Guilard (Academic Press, San Diego, 2000)